

Intrinsic antiferromagnetic topological insulator and axion state in V_2WS_4

Yadong Jiang,¹ Huan Wang,¹ Kejie Bao,¹ and Jing Wang^{1, 2, 3, *}

¹State Key Laboratory of Surface Physics and Department of Physics, Fudan University, Shanghai 200433, China

²Institute for Nanoelectronic Devices and Quantum Computing, Fudan University, Shanghai 200433, China

³Zhangjiang Fudan International Innovation Center, Fudan University, Shanghai 201210, China

(Dated: August 30, 2023)

Intrinsic magnetic topological insulators offers an ideal platform to explore exotic topological phenomena, such as axion electrodynamics, quantum anomalous Hall (QAH) effect and Majorana edge modes. However, these emerging new physical effects have rarely been experimentally observed due to the limited choice of suitable materials. Here, we predict the van der Waals layered V_2WS_4 and its related materials show intralayer ferromagnetic and interlayer antiferromagnetic exchange interactions. We find extremely rich magnetic topological states in V_2WS_4 , including an antiferromagnetic topological insulator, the axion state with the long-sought quantized topological magnetoelectric effect, three-dimensional QAH state, as well as a collection of QAH insulators and intrinsic axion insulators in odd- and even-layer films, respectively. Remarkably, the Néel temperature of V_2WS_4 is predicted to be much higher than that of $MnBi_2Te_4$. These interesting predictions, if realized experimentally, could greatly promote the topological quantum physics research and application.

The discovery of intrinsically magnetic topological insulators (TI) [1–6] brings the opportunity to realize a large family of exotic topological phenomena through the time-reversal-breaking topological surface states [7–33]. A paradigm example is the realization of the quantum anomalous Hall (QAH) effect and axion insulator in few layer $MnBi_2Te_4$ [34–40]. The study of magnetic topological states falls much behind in experiments compared to non-magnetic counterparts due to the limited choice of magnetic TI materials. Though hundreds of intrinsic magnetic topological materials have been identified by symmetry-based analysis [41–46] and *ab initio* calculations [47], the vast majority of them are semimetals. The only experimental confirmed intrinsic antiferromagnetic (AFM) TI is $MnBi_2Te_4$ [37, 38]. However, the Néel temperature of $MnBi_2Te_4$ is relatively low, and the complex magnetic structure and imperfect sample quality may be responsible for the lack of direct observation of the exchange gap of Dirac surface states in spectroscopy measurements [38, 48–50]. Therefore, realistic intrinsic magnetic TI materials preferably with high magnetically ordered temperature are highly desired. The class of V_2WS_4 materials predicted in this paper have high Néel temperature and provide an ideal platform for emergent magnetic topological phenomena, such as AFM TI, topological axion state with topological magnetoelectric effect (TME), QAH effect in both two- and three-dimensions (3D), and so on.

Structure and magnetic properties. The ternary transition metal chalcogenide V_2MX_4 , with $M = W$ or Mo , $X = S$ or Se , crystallize in an orthorhombic crystal structure with the space group $I\bar{4}2m$ (No. 121) with seven atoms in one primitive cell. We take V_2WS_4 as an example. It has a layered structure with a tetragonal lattice V_2WS_4 as the building block shown in Fig. 1. The key symmetry operation is $\mathcal{I}C_{4z}$, where \mathcal{I} is inversion symmetry. Each layer contains three atomic layers (i.e. one

V_2W and two S_2), where each V or W atom is surrounded by four S atoms forming a distorted edge-sharing tetrahedron. The layers of bulk V_2WS_4 are connected by van der Waals interactions and stack along z axis, forming an AB stacking pattern, which is energetically favorable than AA stacking. The B layer can be regard as A layer translating along $\tau_{1/2} = (a, a, c)/2$, where $(a, c) = (5.79, 9.55)\text{\AA}$ are the in-plane and out-of plane lattice constant, respectively. The dynamical stability of V_2WS_4 is confirmed by first-principles phonon calculations [51]. Moreover, Cu_2MX_4 and Ag_2MX_4 with the same structure have been successfully synthesized [52–55], implying that these

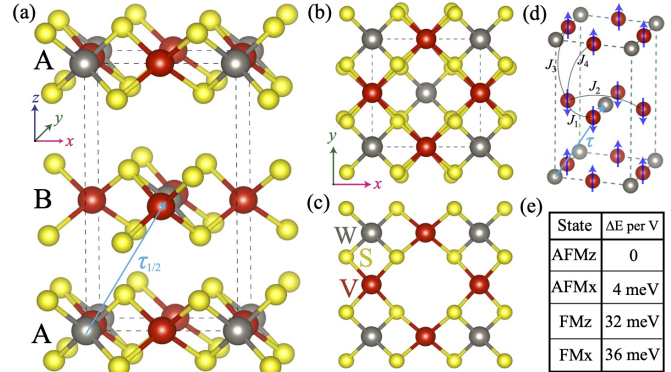


FIG. 1. Crystal and magnetic structures. (a) The unit cell of AFM V_2WS_4 consists of two layers with AB stacking. The cyan arrow denotes for the half translation operator $\tau_{1/2}$. (b) The top view along the z axis. (c) The monolayer atomic structure from top view. (d) The magnetic AFM-z ground state. J_i denote the leading magnetic couplings between V-V pairs, and negative J_i means FM exchange coupling. $J_1 = -13.0$ meV, $J_2 = -7.5$ meV only represents intralayer next-nearest-neighbor V-V pairs through W atoms, $J_3 = 1.7$ meV, $J_4 = 1.4$ meV. (e) The calculated total energy for different magnetic ordered states.

materials could possibly be fabricated by experiment.

First-principles density functional theory (DFT) calculations are employed to investigate the electronic structure of V_2WS_4 , where the detailed methods can be found in Supplementary Material [51]. We find each V atom has a valence of +2 by losing its two $4s$ electrons. We performed total energy calculations for different magnetic structures for 3D V_2WS_4 , and the results are listed in Fig. 1(e), showing that A -type AFM state with out-of-plane easy axis (denoted as AFM- z) is the magnetic ground state. It is FM within xy plane in each layer, and AFM between adjacent layers along z direction (Fig. 1(d)). The total energy of A -type AFM state with in-plane easy axis (AFM- x) is slightly higher than that of AFM- z , but much lower than FM- z state with an out-of-plane easy axis, which indicates that magnetic anisotropy energy is weaker than the effective magnetic exchange interaction between neighboring layers. The calculated magnetic moments are mainly contributed by V ($\approx 2.6\mu_B$) rather than W ($\approx 0.4\mu_B$), thus the magnetism is from V atoms. Such a fractional magnetic moment is due to the band inversion between V $d_{xz,yz}$ orbitals and W d_{z^2} orbital (Fig. 2(a)). The tetrahedral crystal field splits V $3d$ orbitals into $e_g(d_{z^2}, d_{x^2-y^2})$ and triplet $t_{2g}(d_{xz/yz}, d_{xy})$, where the energy of e_g stays lower with respect to t_{2g} . The remaining three $3d$ electrons fill up the spin-up V- d levels in the $e_g^2t_{2g}^1$ configuration with $3\mu_B$ magnetic moment according to the Hund's rule, which is close to the DFT calculation. The FM exchange coupling between neighboring V atoms within each layer is strongly enhanced by Hund's rule interaction due to empty t_{2g} orbitals [56]. The t_{2g} - t_{2g} super-exchange of V atoms between neighbor layers via p orbitals of ligand is AFM due to the Goodenough-Kanamori-Anderson rule [56]. Furthermore, the Néel temperature for AFM- z V_2WS_4 is estimated as 510 K by Monte Carlo simulations [51].

AFM TI and topological invariant. First we investigate the AFM- z ground state. It has the type IV magnetic space group No. 114.282 as in Belov-Neronova-Smirnova (BNS) notation [57], where the symmetry generators include \mathcal{IC}_{4z} , $\Theta\tau_{1/2}$, C_{2z} and $C_{2x}\tau_{1/2}$. The time-reversal symmetry Θ is broken; however, a combined symmetry $\mathcal{S} \equiv \Theta\tau_{1/2}$ is preserved, where $\tau_{1/2}$ is the half translation operator connecting neighboring W atomic layers, marked in Fig. 1(a). \mathcal{S} is antiunitary with $\mathcal{S}^2 = -e^{-2i\mathbf{k}\cdot\tau_{1/2}}$. $\mathcal{S}^2 = -1$ on Brillouin-zone (BZ) plane

K	$\Gamma(000)$	$M(\pi\pi 0)$	$Z(00\pi)$	$A(\pi\pi\pi)$
$n_K^{1/2}, n_K^{-3/2}$	20, 20	20, 20	20, 20	19, 21

TABLE I. The number of occupied bands with \mathcal{IC}_{4z} eigenvalue $e^{-i\frac{\pi}{4}}$ and $e^{i\frac{3\pi}{4}}$ at four high symmetry points in BZ.

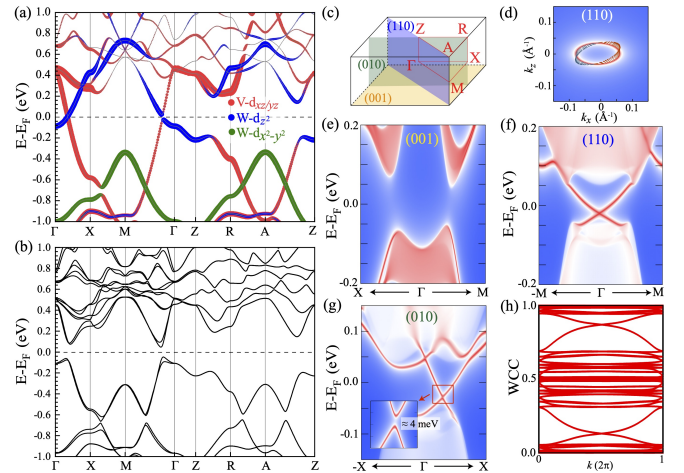


FIG. 2. Electronic structure and surfaces states of AFM- z V_2WS_4 . (a) The d -orbitals projected band structure without SOC, only those bands which are related to band inversion are highlighted. (b) Band structure with SOC. (c) Brillouin zone. (110), (001), and (001) surfaces are labeled as blue, orange, and green, respectively. (d) Fermi surface with spin texture on the (110) surface at Fermi level presents an ellipse shape. Blue and orange arrow of spin texture denote $s_y < 0$ and $s_y > 0$, respectively. (e)-(g) Surface states of the semi-infinite (001), (110) and (010) surfaces, respectively, which is gapless on the \mathcal{S} -preserving (110) surface, but gapped on the \mathcal{S} -broken (001) and (010) surfaces. (h) The Wannier charge centers (WCC) is calculated in the plane including TRI momenta (000) , $(\pi\bar{\pi}0)$, $(\pi0\bar{\pi})$, and $(0\pi\bar{\pi})$ with $\mathbf{k} \cdot \tau_{1/2} = 0$, confirming $\mathcal{Z}_2 = 1$.

$\mathbf{k} \cdot \tau_{1/2} = 0$. Therefore, similar to Θ in time-reversal-invariant (TRI) TI, \mathcal{S} could also lead a \mathcal{Z}_2 classification [18], where the \mathcal{Z}_2 topological invariant is well defined on the BZ plane with $\mathbf{k} \cdot \tau_{1/2} = 0$. The electronic structure without and with spin-orbital coupling (SOC) are shown in Fig. 2(a) and Fig. 2(b), respectively. One can see an anticrossing feature around Γ point from the band inversion between V $d_{xz,yz}$ orbitals and W d_{z^2} orbital, suggesting that V_2WS_4 might be topologically nontrivial. Since \mathcal{I} is broken but \mathcal{IC}_{4z} is preserved, the \mathcal{Z}_2 invariant is simply determined by the \mathcal{IC}_{4z} eigenvalues of the wavefunctions at \mathcal{IC}_{4z} -invariant momenta in the BZ [43], with the explicit form

$$\mathcal{Z}_2 = \sum_{K=\Gamma, M, Z, A} \frac{1}{2} \left(n_K^{\frac{1}{2}} - n_K^{-\frac{3}{2}} \right) \bmod 2, \quad (1)$$

where $n_K^{1/2}$ and $n_K^{-3/2}$ are the number of occupied states with \mathcal{IC}_{4z} eigenvalues $e^{-i\pi/4}$ and $e^{i3\pi/4}$, respectively. $K = \Gamma, M, Z, A$ are \mathcal{IC}_{4z} invariant in BZ. $n_K^{1/2}$ and $n_K^{-3/2}$ of high symmetry points are listed in Table I, so $\mathcal{Z}_2 = 1$. There are two other symmetry indicators \mathcal{Z}_4 and δ_2 , the nonzero value of which characterize higher-order topology and Weyl semimetal [58, 59]. Here $\mathcal{Z}_4 = \delta_2 = 0$, because the Chern number of all k_z planes in BZ is always equal to zero. The monolayer is a FM QAH insu-

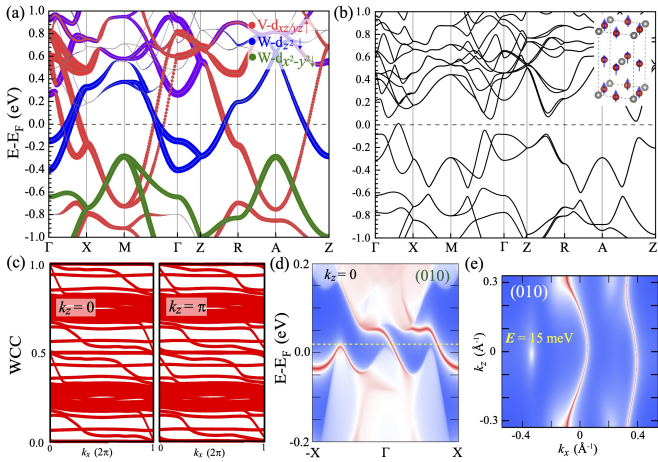


FIG. 3. Electronic structure and surfaces states of FM- z V_2WS_4 . (a) The d -orbital projected band structure without SOC. (b) Band structure with SOC. Here the conventional unit cell with FM- z state is chosen. (c) The evolution of WCC along the k_x direction in the $k_z = 0$ and $k_z = \pi$ plane. (d) Two chiral surface states on the semi-infinite (010) surface at $k_z = 0$. Consistent with WCC in (c), the Chern number is $\mathcal{C} = -2$ from $k_z = 0$ to $k_z = \pi$. (e) Fermi surface on the (010) termination at the isoenergy 15 meV above Fermi level. The chiral surface states extend over the entire surface BZ from $k_z = -\pi$ to $k_z = \pi$, indicating the 3D QAH state.

lator [60], thus 3D AFM- z V_2WS_4 is successive stacking of layered QAH with alternating Chern number $\mathcal{C} = \pm 1$, which is related by \mathcal{S} symmetry. We further employ the Willson loop method [61] to confirm the \mathcal{Z}_2 invariant in Fig. 2(h), concluding that AFM- z V_2WS_4 is an AFM TI. Especially, we notice that a large energy gap of about 0.1 eV is obtained in Fig. 2(b).

One prominent feature of AFM TI is the existence of gapless surface states that depends on the surface plane, which is confirmed by the surface-state calculations. As shown in Fig. 2(f), the gapless surface states can be seen at Γ point forming a single Dirac cone in bulk gap on \mathcal{S} -preserving (110) surface. While the surface states are gapped on \mathcal{S} -broken (001) and (010) surfaces, as shown in Fig. 2(e) and Fig. 2(g).

Axion state and TME. The $\mathcal{Z}_2 = 1$ topological invariant of AFM- z V_2WS_4 with a full band gap indicates the axion state with a quantized value $\theta = \pi \pmod{2\pi}$, where the electromagnetic response is described by the axion electrodynamics, $S_\theta = (\theta/2\pi)(\alpha/2\pi) \int d^3x dt \mathbf{E} \cdot \mathbf{B}$. Here, \mathbf{E} and \mathbf{B} are the conventional electromagnetic fields inside the insulator, $\alpha = e^2/\hbar c$ is the fine-structure constant, e is electron charge, and θ is dimensionless pseudoscalar parameter [7]. Such an axion state exhibits TME, which has not been experimentally observed [3]. Interestingly, the gapped surface states from time-reversal symmetry breaking are naturally and intrinsically provided by even-layer V_2WS_4 films with A -type AFM structure, which make it an ideal platform for

the long-sought quantized TME. Furthermore, to observe TME, all surface states must be gapped [22], which could be fulfilled by growing realistic materials without any \mathcal{S} -preserving surfaces. Compared to the previous proposals on TME in FM-TI heterostructure [7, 22, 23], the intrinsic magnetic TI material V_2WS_4 could greatly facilitate the study of axion electrodynamics.

3D QAH state. The AFM ground state of V_2WS_4 could be tuned to FM configuration by applying an external magnetic field, which further leads to distinct topological phases. Here we study FM- z state, which belongs to magnetic space group No. 121.331 in BNS notation with symmetry generators \mathcal{IC}_{4z} , C_{2z} and ΘC_{2y} . For simplicity, we adopted the conventional unit cell here as in AFM- z state. Then 3D FM- z V_2WS_4 can be viewed as layer stacking of FM QAH insulator with the same Chern number $\mathcal{C} = -1$, leading to 3D QAH state or Weyl semimetal [62, 63]. The electronic structures without and with SOC are calculated in Fig. 3(a) and Fig. 3(b), respectively. There is spin polarized band inversion near the Fermi energy between spin up d_{xz}, d_{yz} bands of V and spin down d_{z^2} band of W, which is further gapped by SOC. Interestingly, along Γ -Z line, the band inversion always remains and there is no level crossing. Meanwhile, FM- z state is full insulating with a gap of about 20 meV. The Willson loop calculations in Fig. 3(c) found that the Chern number $\mathcal{C} = -2$ at both $k_z = 0$ and $k_z = \pi$ planes, indicating that the system is a 3D QAH state. Moreover, our surface state calculations demonstrated the existence of chiral surface state on the (010) termination, which is the fingerprint of 3D QAH state. As shown in Fig. 3(d), two chiral edge states disperse within the bulk gap at $k_z = 0$ plane. Such chiral edge states extend over the entire surface BZ from $k_z = -\pi$ to $k_z = \pi$ plane without any Weyl points (Fig. 3(e)). Thin films of 3D QAH insulator lead to the QAH effect in 2D, the Chern number of which is equal to the layer number as will be discussed later. The high Chern number QAH effect with multiple dissipationless edge channels could lead to novel design of low energy cost electronic devices.

Tight-binding model and multilayer. The layered van der Waals materials are featured by tunable quantum size effects. Here the band inversion in 3D suggests nontrivial topology may also exist in 2D multilayers. For AFM V_2WS_4 films, even layers have \mathcal{IC}_{4z} and $C_{2x}\tau'_{1/2}$ symmetries, $\tau'_{1/2} \equiv (a, a, 0)/2$. All of the bands have Chern number $\mathcal{C} = 0$ because of the Hall conductance σ_{xy} is odd under $C_{2x}\tau'_{1/2}$. Differently, odd layers have \mathcal{IC}_{4z} and $C_{2x}\Theta$ symmetries, $\mathcal{C} \neq 0$ is allowed for σ_{xy} is invariant under $C_{2x}\Theta$. We construct a tight-binding model to recover the essential topological physics for AFM ground state, and investigate the crossover between bulk and multilayers.

From DFT calculations in Fig. 2, we construct the minimal tight-binding model including d_{xz}, d_{yz} of V and $d_{z^2}, d_{x^2-y^2}$ of W, where the band gap is mainly pro-

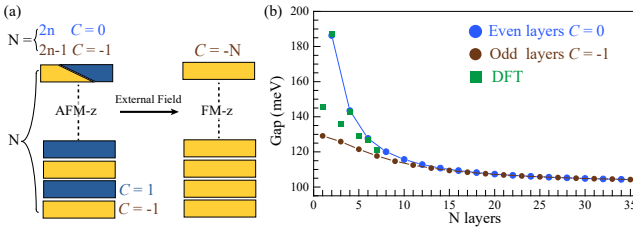


FIG. 4. (a) Schematic diagram shows layered stacking of QAH insulators with alternating Chern number $\mathcal{C} = \pm 1$. In AFM- z state, it gives $\mathcal{C} = -1$ QAH insulator in odd layers and $\mathcal{C} = 0$ axion insulator in even layers. In FM- z state viewed as stacking of same Chern number $\mathcal{C} = -1$ QAH insulators, N layers is a $\mathcal{C} = -N$ high Chern number QAH insulator. (b) The evolution of band gap as a function of layer number in AFM- z state. Blue (brown) circle denotes even (odd) layers calculated from tight-binding model. Green box represents the gaps in one to seven layers by DFT calculations.

vided by the intralayer SOC effect with the opposite spin and interlayer orbital hopping with the same spin. The Hamiltonian is written as $\mathcal{H} = \begin{pmatrix} \mathcal{H}_1 & \mathcal{T} \\ \mathcal{T}^\dagger & \mathcal{H}_2 \end{pmatrix}$, where $\mathcal{H}_{1,2}$ are the intralayer Hamiltonian for two layers in the unit cell, \mathcal{T} is the interlayer hopping. For the intralayer, d_{xz} from one V and d_{yz} from the other V are degenerate, which are related to each other by $\mathcal{I}\mathcal{C}_{4z}$. Then we construct four orbital model for the low energy physics in one layer as $\mathcal{H}_1 = \sum_i d_{1,i}^\dagger \varepsilon_0^i d_{1,i} + \sum_{\langle ij \rangle} [d_{1,i}^\dagger \hat{t}_{ij} d_{1,j} + \text{H.c.}] + \sum_{\langle\langle ij \rangle\rangle} [d_{1,i}^\dagger \hat{t}'_{ij} d_{1,j} + \text{H.c.}]$, where $\langle ij \rangle$ and $\langle\langle ij \rangle\rangle$ denote the nearest-neighbor and next-nearest-neighbor sites, respectively, $d_1 \equiv (d_{1,xz}^\dagger, d_{1,yz}^\dagger, d_{1,zz}^\dagger, d_{1,x^2-y^2}^\dagger)^T$, ε_0^i is the on-site energy, \hat{t}_{ij} and \hat{t}'_{ij} are 4×4 hopping matrices terms with SOC included, which can be simplified by symmetry considerations. \mathcal{H}_2 of other layer is related to \mathcal{H}_1 by \mathcal{S} symmetry, where the spins are flipped with the basis of $d_2 \equiv (d_{2,xz}^\dagger, d_{2,yz}^\dagger, d_{2,zz}^\dagger, d_{2,x^2-y^2}^\dagger)^T$. The interlayer hopping includes the orbital overlapping with the same spin $\mathcal{T} = \sum_{\langle ij \rangle} d_{1,i}^\dagger \hat{s}_{ij} d_{2,j}$, with the strength of about 50 meV which is smaller than the intralayer SOC. The explicit forms and fitted parameters are listed in Supplementary Materials, where similar electronic structure and surface states of our model are obtained as DFT calculations [51].

By utilizing the tight-binding model, we can study the dimensional crossover from bulk to multilayer. As shown in Fig. 4, in AFM- z ground state, the band gap of multilayer shows oscillatory decay behavior and gradually converges to bulk value when the film exceed twenty layers, while the Chern number exhibit pronounced even-odd oscillations. The Chern number of band in a $\mathcal{I}\mathcal{C}_{4z}$ invariant system is $i^{\mathcal{C}} = \prod_{j \in \text{occupied}} (-1)^F \xi_j(\Gamma) \xi_j(M) \xi_j(X)$, with $F = 0$ or 1 labels spinless or spinful case, respectively, $\xi_j(k)$ is the $\mathcal{I}\mathcal{C}_{4z}$ eigenvalue at Γ and M points of the j -th band, $\xi_j(X)$ is the C_{2z} eigenvalue at X point on the j -th band [60]. Explicitly, odd layers have $\mathcal{C} = -1$, while even

layers have $\mathcal{C} = 0$. Our DFT calculations up to seven layers are consistent with effective model [51]. These results suggest that multilayer V_2WS_4 can be viewed as layered stacking of alternating $\mathcal{C} = \pm 1$ QAH insulators for AFM state, or stacking of same $\mathcal{C} = -1$ QAH insulators for FM state, as illustrated in Fig. 4(a). The interlayer coupling is weaker than band inversion and SOC, thus the Chern number of multilayer is simply the summation of Chern number from each layer, namely

$$\mathcal{C}_{\text{multilayer}} = \sum_j \mathcal{C}_j. \quad (2)$$

Here $\mathcal{C}_j = \pm 1$ for each layer is only determined by the direction of magnetic moment, and does not affected by interlayer coupling.

It is interesting to compare V_2WS_4 with MnBi_2Te_4 . Both materials are layered van der Waals intrinsic magnetic TI with similar topological properties. In the AFM ground state, they are AFM TI and axion state in 3D, and display oscillation between even and odd Chern numbers in AFM multilayers. The main difference lies in FM- z state. While V_2WS_4 is a 3D QAH state, MnBi_2Te_4 tends to be Weyl semimetal or trivial FM insulator [35, 36]. The underlying reasons are attributed to the interlayer coupling and band inversion. First, the low energy physics in V_2WS_4 is from the d -orbitals of V and W located in the middle atomic layer, as opposed to the p_z orbitals of outermost Bi/Te atom layers in MnBi_2Te_4 layer. Therefore, the interlayer coupling is indirect and smaller in V_2WS_4 compared to MnBi_2Te_4 (about 0.1 eV). Second, V_2WS_4 possesses much deeper band inversion. The band inversion points lie approximately at 35% along Γ -X line from Γ ($|\mathbf{k}| = 0.19 \text{ \AA}^{-1}$) as shown in Fig. 2(a), which is further opened by a strong SOC. Therefore weak interlayer coupling could not change the band inversion along Γ -Z in V_2WS_4 . While the SOC induced band inversion is at Γ in MnBi_2Te_4 , thus the comparable interlayer coupling could modify the band inversion and lead to trivial insulators in few layers and Weyl semimetal in 3D. We conclude that such characteristics do not arise from fortuitousness in parameters, but rather from the universality inherent in V_2WS_4 family.

Discussion. Other ternary transition metal chalcogenide V_2WSe_4 , V_2MoX_4 , V_2TaX_4 and Ti_2WX_4 ($X = \text{S}$ or Se), if with the same orthorhombic crystal structure, are also promising candidates to host magnetic topological states similar to V_2WS_4 . Actually, most of them are AFM TI in the ground state calculated in Supplementary Materials [51]. The synergy between intrinsic magnetism and topological bands, together with the rich choices of candidate materials, open a broad way to study rich emergent phenomena of magnetic topological states in different spatial dimensions. For example, the magnetic fluctuations in these systems also give dynamic axion field.

The field of topological quantum matter in recent years developed explosively in materials science and condensed matter physics. One of main reasons is the precise theoretical predictions and experimental discovery of intrinsic topological materials. Tracing back the research history in magnetic topological physics, most of the previous experimental works are based on magnetically doped TIs and heterostructures [13–17, 24–27], which are quite complex and challenge to study [64, 65]. The research progress have been greatly prompted by discovering intrinsic magnetic TI material MnBi_2Te_4 [34, 39]. However, the co-antisite defects in Mn and Bi layers drastically suppress the exchange gap by several order of magnitude [66, 67], which fundamentally deteriorates magnetic topological states. Meanwhile, few layers MnBi_2Te_4 with topologically nontrivial bands are too thick to tune efficiently. Finally, layered MnBi_2Te_4 usually contain Bi_2Te_3 layers, which further complicates the electronic structure with undesired topology. The V_2WS_4 -family materials satisfy all these material characteristics of simple, magnetic and topological. For example, monolayer V_2WS_4 is QAH insulator, in contrast to trivial FM insulator of monolayer MnBi_2Te_4 . Therefore, the techniques developed for 2D materials with versatile tunability can be readily applied to V_2WS_4 family. We anticipate that van der Waals heterostructures integrating V_2WS_4 family with other magnetic or superconducting 2D materials will provide fertile ground for exploring exotic topological quantum phenomena.

Acknowledgment. This work is supported by the National Key Research Program of China under Grant No. 2019YFA0308404, the Natural Science Foundation of China through Grant No. 12174066, Science and Technology Commission of Shanghai Municipality under Grant No. 20JC1415900, the Innovation Program for Quantum Science and Technology through Grant No. 2021ZD0302600, Shanghai Municipal Science and Technology Major Project under Grant No. 2019SHZDZX01.

* Corresponding author: wjingphys@fudan.edu.cn

[1] M. Z. Hasan and C. L. Kane, “Colloquium: Topological insulators,” *Rev. Mod. Phys.* **82**, 3045–3067 (2010).

[2] Xiao-Liang Qi and Shou-Cheng Zhang, “Topological insulators and superconductors,” *Rev. Mod. Phys.* **83**, 1057–1110 (2011).

[3] Yoshinori Tokura, Kenji Yasuda, and Atsushi Tsukazaki, “Magnetic topological insulators,” *Nature Rev. Phys.* **1**, 126–143 (2019).

[4] Jing Wang and Shou-Cheng Zhang, “Topological states of condensed matter,” *Nature Mat.* **16**, 1062–1067 (2017).

[5] B. Andrei Bernevig, Claudia Felser, and Haim Beidenkopf, “Progress and prospects in magnetic topological materials,” *Nature* **603**, 41–51 (2022).

[6] Cui-Zu Chang, Chao-Xing Liu, and Allan H. MacDonald, “Colloquium: Quantum anomalous hall effect,” *Rev. Mod. Phys.* **95**, 011002 (2023).

[7] Xiao-Liang Qi, Taylor L. Hughes, and Shou-Cheng Zhang, “Topological field theory of time-reversal invariant insulators,” *Phys. Rev. B* **78**, 195424 (2008).

[8] Andrew M. Essin, Joel E. Moore, and David Vanderbilt, “Magnetoelectric polarizability and axion electrodynamics in crystalline insulators,” *Phys. Rev. Lett.* **102**, 146805 (2009).

[9] Xiao-Liang Qi, Rundong Li, Jiadong Zang, and Shou-Cheng Zhang, “Seeing the magnetic monopole through the mirror of topological surface states,” *Science* **323**, 1184 (2009).

[10] Y. L. Chen, J.-H. Chu, J. G. Analytis, Z. K. Liu, K. Igarashi, H.-H. Kuo, X. L. Qi, S. K. Mo, R. G. Moore, D. H. Lu, M. Hashimoto, T. Sasagawa, S. C. Zhang, I. R. Fisher, Z. Hussain, and Z. X. Shen, “Massive dirac fermion on the surface of a magnetically doped topological insulator,” *Science* **329**, 659–662 (2010).

[11] Rundong Li, Jing Wang, X. L. Qi, and S. C. Zhang, “Dynamical axion field in topological magnetic insulators,” *Nature Phys.* **6**, 284 (2010).

[12] Rui Yu, Wei Zhang, Hai-Jun Zhang, Shou-Cheng Zhang, Xi Dai, and Zhong Fang, “Quantized Anomalous Hall Effect in Magnetic Topological Insulators,” *Science* **329**, 61–64 (2010).

[13] Cui-Zu Chang, Jinsong Zhang, Xiao Feng, Jie Shen, Zuocheng Zhang, Minghua Guo, Kang Li, Yunbo Ou, Pang Wei, Li-Li Wang, Zhong-Qing Ji, Yang Feng, Shuaihua Ji, Xi Chen, Jinfeng Jia, Xi Dai, Zhong Fang, Shou-Cheng Zhang, Ke He, Yayu Wang, Li Lu, Xu-Cun Ma, and Qi-Kun Xue, “Experimental Observation of the Quantum Anomalous Hall Effect in a Magnetic Topological Insulator,” *Science* **340**, 167–170 (2013).

[14] J. G. Checkelsky, R. Yoshimi, A. Tsukazaki, K. S. Takahashi, Y. Kozuka, J. Falson, M. Kawasaki, and Y. Tokura, “Trajectory of the anomalous hall effect towards the quantized state in a ferromagnetic topological insulator,” *Nature Phys.* **10**, 731 (2014).

[15] Xufeng Kou, Shih-Ting Guo, Yabin Fan, Lei Pan, Murong Lang, Ying Jiang, Qiming Shao, Tianxiao Nie, Koichi Murata, Jianshi Tang, Yong Wang, Liang He, Ting-Kuo Lee, Wei-Li Lee, and Kang L. Wang, “Scale-invariant quantum anomalous hall effect in magnetic topological insulators beyond the two-dimensional limit,” *Phys. Rev. Lett.* **113**, 137201 (2014).

[16] A. J. Bestwick, E. J. Fox, Xufeng Kou, Lei Pan, Kang L. Wang, and D. Goldhaber-Gordon, “Precise quantization of the anomalous hall effect near zero magnetic field,” *Phys. Rev. Lett.* **114**, 187201 (2015).

[17] Cui-Zu Chang, Weiwei Zhao, Duk Y. Kim, Haijun Zhang, Badih A. Assaf, Don Heiman, Shou-Cheng Zhang, Chaoxing Liu, Moses H. W. Chan, and Jagadeesh S. Moodera, “High-precision realization of robust quantum anomalous hall state in a hard ferromagnetic topological insulator,” *Nature Mater.* **14**, 473 (2015).

[18] Roger S. K. Mong, Andrew M. Essin, and Joel E. Moore, “Antiferromagnetic topological insulators,” *Phys. Rev. B* **81**, 245209 (2010).

[19] Xiangang Wan, Ari M. Turner, Ashvin Vishwanath, and Sergey Y. Savrasov, “Topological semimetal and fermi-arc surface states in the electronic structure of pyrochlore iridates,” *Phys. Rev. B* **83**, 205101 (2011).

[20] Gang Xu, Hongming Weng, Zhijun Wang, Xi Dai, and Zhong Fang, “Chern Semimetal and the Quantized Anomalous Hall Effect in HgCr_2Se_4 ,” *Phys. Rev. Lett.* **107**, 186806 (2011).

[21] Kentaro Nomura and Naoto Nagaosa, “Surface-quantized anomalous hall current and the magnetoelectric effect in magnetically disordered topological insulators,” *Phys. Rev. Lett.* **106**, 166802 (2011).

[22] Jing Wang, Biao Lian, Xiao-Liang Qi, and Shou-Cheng Zhang, “Quantized topological magnetoelectric effect of the zero-plateau quantum anomalous Hall state,” *Phys. Rev. B* **92**, 081107 (2015).

[23] Takahiro Morimoto, Akira Furusaki, and Naoto Nagaosa, “Topological magnetoelectric effects in thin films of topological insulators,” *Phys. Rev. B* **92**, 085113 (2015).

[24] M. Mogi, M. Kawamura, R. Yoshimi, A. Tsukazaki, Y. Kozuka, N. Shirakawa, K. S. Takahashi, M. Kawasaki, and Y. Tokura, “A magnetic heterostructure of topological insulators as a candidate for an axion insulator,” *Nature Mater.* **16**, 516–521 (2017).

[25] Masataka Mogi, Minoru Kawamura, Atsushi Tsukazaki, Ryutaro Yoshimi, Kei S. Takahashi, Masashi Kawasaki, and Yoshinori Tokura, “Tailoring tricolor structure of magnetic topological insulator for robust axion insulator,” *Sci. Adv.* **3**, eaao1669 (2017).

[26] S. Grauer, K. M. Fijalkowski, S. Schreyeck, M. Winnerlein, K. Brunner, R. Thomale, C. Gould, and L. W. Molenkamp, “Scaling of the quantum anomalous hall effect as an indicator of axion electrodynamics,” *Phys. Rev. Lett.* **118**, 246801 (2017).

[27] Di Xiao, Jue Jiang, Jae-Ho Shin, Wenbo Wang, Fei Wang, Yi-Fan Zhao, Chaoxing Liu, Weida Wu, Moses H. W. Chan, Nitin Samarth, and Cui-Zu Chang, “Realization of the Axion Insulator State in Quantum Anomalous Hall Sandwich Heterostructures,” *Phys. Rev. Lett.* **120**, 056801 (2018).

[28] Liang Fu and C. L. Kane, “Superconducting proximity effect and majorana fermions at the surface of a topological insulator,” *Phys. Rev. Lett.* **100**, 096407 (2008).

[29] Liang Fu and C. L. Kane, “Probing neutral majorana fermion edge modes with charge transport,” *Phys. Rev. Lett.* **102**, 216403 (2009).

[30] Xiao-Liang Qi, Taylor L. Hughes, and Shou-Cheng Zhang, “Chiral topological superconductor from the quantum hall state,” *Phys. Rev. B* **82**, 184516 (2010).

[31] Jing Wang, Quan Zhou, Biao Lian, and Shou-Cheng Zhang, “Chiral topological superconductor and half-integer conductance plateau from quantum anomalous hall plate transition,” *Phys. Rev. B* **92**, 064520 (2015).

[32] Biao Lian, Xiao-Qi Sun, Abolhassan Vaezi, Xiao-Liang Qi, and Shou-Cheng Zhang, “Topological quantum computation based on chiral majorana fermions,” *Proc. Natl. Acad. Sci. USA* **115**, 10938–10942 (2018).

[33] Jing Wang and Biao Lian, “Multiple chiral majorana fermion modes and quantum transport,” *Phys. Rev. Lett.* **121**, 256801 (2018).

[34] Yujun Deng, Yijun Yu, Meng Zhu Shi, Zhongxun Guo, Zihan Xu, Jing Wang, Xian Hui Chen, and Yuanbo Zhang, “Quantum anomalous hall effect in intrinsic magnetic topological insulator mnbi_2te_4 ,” *Science* **367**, 895–900 (2020).

[35] Dongqin Zhang, Minji Shi, Tongshuai Zhu, Dingyu Xing, Haijun Zhang, and Jing Wang, “Topological axion states in the magnetic insulator mnbi_2te_4 with the quantized magnetoelectric effect,” *Phys. Rev. Lett.* **122**, 206401 (2019).

[36] Jiaheng Li, Yang Li, Shiqiao Du, Zun Wang, Bing-Lin Gu, Shou-Cheng Zhang, Ke He, Wenhui Duan, and Yong Xu, “Intrinsic magnetic topological insulators in van der waals layered mnbi_2te_4 -family materials,” *Sci. Adv.* **5**, eaaw5685 (2019).

[37] Mikhail M. Otrokov, Ilya I. Klimovskikh, Hendrik Bentmann, Alexander Zeugner, Ziya S. Aliev, Sebastian Gass, Anja U. B. Wolter, Alexander V. Koroleva, Dmitry Estyunin, Alexander M. Shikin, María Blanco-Rey, Martin Hoffmann, Alexander Yu. Vyazovskaya, Sergey V. Eremin, Yury M. Koroteev, Imamaddin R. Amiraslanov, Mohammad B. Babanly, Nazim T. Mamedov, Nadir A. Abdullayev, Vladimir N. Zverev, Bernd Büchner, Eike F. Schwier, Shiv Kumar, Akio Kimura, Luca Petaccia, Giovanni Di Santo, Raphael C. Vidal, Sonja Schatz, Katharina Kißner, Chul-Hee Min, Simon K. Moser, Thiago R. F. Peixoto, Friedrich Reinert, Arthur Ernst, Pedro M. Echenique, Anna Isaeva, and Evgeni V. Chulkov, “Prediction and observation of an antiferromagnetic topological insulator,” *Nature* **576**, 416–422 (2019).

[38] Yan Gong, Jingwen Guo, Jiaheng Li, Kejing Zhu, Menghan Liao, Xiaozhi Liu, Qinghua Zhang, Lin Gu, Lin Tang, Xiao Feng, Ding Zhang, Wei Li, Canli Song, Lili Wang, Pu Yu, Xi Chen, Yayu Wang, Hong Yao, Wenhui Duan, Yong Xu, Shou-Cheng Zhang, Xucun Ma, Qi-Kun Xue, and Ke He, “Experimental realization of an intrinsic magnetic topological insulator,” *Chin. Phys. Lett.* **36**, 076801 (2019).

[39] Chang Liu, Yongchao Wang, Hao Li, Yang Wu, Yaxin Li, Jiaheng Li, Ke He, Yong Xu, Jinsong Zhang, and Yayu Wang, “Robust axion insulator and chern insulator phases in a two-dimensional antiferromagnetic topological insulator,” *Nature Mater.* **19**, 522–527 (2020).

[40] Haiming Deng, Zhiyi Chen, Agnieszka Wołos, Marcin Konczykowski, Kamil Sobczak, Joanna Sitnicka, Irina V. Fedorchenco, Jolanta Borysiuk, Tristan Heider, Lukasz Pluciński, Kyungwha Park, Alexandru B. Georgescu, Jennifer Cano, and Lia Krusin-Elbaum, “High-temperature quantum anomalous hall regime in a $\text{mnbi}_2\text{te}_4/\text{bi}_2\text{te}_3$ superlattice,” *Nature Phys.* **17**, 36–42 (2021).

[41] Barry Bradlyn, L Elcoro, Jennifer Cano, MG Vergniory, Zhijun Wang, C Felser, MI Aroyo, and B Andrei Bernevig, “Topological quantum chemistry,” *Nature* **547**, 298 (2017).

[42] Jorrit Kruthoff, Jan de Boer, Jasper van Wezel, Charles L. Kane, and Robert-Jan Slager, “Topological classification of crystalline insulators through band structure combinatorics,” *Phys. Rev. X* **7**, 041069 (2017).

[43] Luis Elcoro, Benjamin J. Wieder, Zhida Song, Yuanfeng Xu, Barry Bradlyn, and B. Andrei Bernevig, “Magnetic topological quantum chemistry,” *Nature Commun.* **12**, 5965 (2021).

[44] Hoi Chun Po, Ashvin Vishwanath, and Haruki Watanabe, “Symmetry-based indicators of band topology in the 230 space groups,” *Nature Commun.* **8**, 50 (2017).

[45] Haruki Watanabe, Hoi Chun Po, and Ashvin Vishwanath, “Structure and topology of band structures in the 1651 magnetic space groups,” *Sci. Adv.* **4**, eaat8685 (2018).

[46] Hoi Chun Po, “Symmetry indicators of band topology,”

J. Phys.: Condens. Matter **32**, 263001 (2020).

[47] Yuanfeng Xu, Luis Elcoro, Zhi-Da Song, Benjamin J. Wieder, M. G. Vergniory, Nicolas Regnault, Yulin Chen, Claudia Felser, and B. Andrei Bernevig, “High-throughput calculations of magnetic topological materials,” *Nature* **586**, 702–707 (2020).

[48] Yu-Jie Hao, Pengfei Liu, Yue Feng, Xiao-Ming Ma, Eike F. Schwier, Masashi Arita, Shiv Kumar, Chaowei Hu, Rui'e Lu, Meng Zeng, Yuan Wang, Zhanyang Hao, Hong-Yi Sun, Ke Zhang, Jiawei Mei, Ni Ni, Liusuo Wu, Kenya Shimada, Chaoyu Chen, Qihang Liu, and Chang Liu, “Gapless surface dirac cone in antiferromagnetic topological insulator mnbi_2te_4 ,” *Phys. Rev. X* **9**, 041038 (2019).

[49] Hang Li, Shun-Ye Gao, Shao-Feng Duan, Yuan-Feng Xu, Ke-Jia Zhu, Shang-Jie Tian, Jia-Cheng Gao, Wen-Hui Fan, Zhi-Cheng Rao, Jie-Rui Huang, Jia-Jun Li, Da-Yu Yan, Zheng-Tai Liu, Wan-Ling Liu, Yao-Bo Huang, Yu-Liang Li, Yi Liu, Guo-Bin Zhang, Peng Zhang, Takeshi Kondo, Shik Shin, He-Chang Lei, You-Guo Shi, Wen-Tao Zhang, Hong-Ming Weng, Tian Qian, and Hong Ding, “Dirac surface states in intrinsic magnetic topological insulators $\text{eus}_{2n}\text{as}_2$ and $\text{mnbi}_{2n}\text{te}_{3n+1}$,” *Phys. Rev. X* **9**, 041039 (2019).

[50] Y. J. Chen, L. X. Xu, J. H. Li, Y. W. Li, H. Y. Wang, C. F. Zhang, H. Li, Y. Wu, A. J. Liang, C. Chen, S. W. Jung, C. Cacho, Y. H. Mao, S. Liu, M. X. Wang, Y. F. Guo, Y. Xu, Z. K. Liu, L. X. Yang, and Y. L. Chen, “Topological electronic structure and its temperature evolution in antiferromagnetic topological insulator mnbi_2te_4 ,” *Phys. Rev. X* **9**, 041040 (2019).

[51] See Supplemental Material for methods and technical details.

[52] Clare J. Crossland, Peter J. Hickey, and John S. O. Evans, “The synthesis and characterisation of cu2mx_4 ($m = w$ or mo ; $x = s$, se or s/se) materials prepared by a solvothermal method,” *J. Mater. Chem.* **15**, 3452–3458 (2005).

[53] Xin Hu, Wei Shao, Xudong Hang, Xiaodong Zhang, Wenguang Zhu, and Yi Xie, “Superior electrical conductivity in hydrogenated layered ternary chalcogenide nanosheets for flexible all-solid-state supercapacitors,” *Angew. Chem. Int. Ed.* **55**, 5733–5738 (2016).

[54] Fengping Zhan, Qinghua Wang, Yibing Li, Xin Bo, Qingxiang Wang, Fei Gao, and Chuan Zhao, “Low-temperature synthesis of cuboid silver tetrathiotungstate (ag_2ws_4) as electrocatalyst for hydrogen evolution reaction,” *Inorg. Chem.* **57**, 5791–5800 (2018).

[55] Yunxiang Lin, Shuangming Chen, Ke Zhang, and Li Song, “Recent advance of ternary layered cu2mx_4 ($m=mo$, w ; $x=s$, se) nanomaterials for photocatalysis,” *Solar RRL* **3**, 1800320 (2019).

[56] Daniel I. Khomskii, *Transition Metal Compounds* (Cambridge University Press, 2004).

[57] C. J. Bradley and A. P. Cracknell, *The Mathematical Theory of Symmetry in Solids* (Clarendon Press, Oxford, 1972).

[58] Zhida Song, Tiantian Zhang, Zhong Fang, and Chen Fang, “Quantitative mappings between symmetry and topology in solids,” *Nature Commun.* **9**, 3530 (2018).

[59] Eslam Khalaf, Hoi Chun Po, Ashvin Vishwanath, and Haruki Watanabe, “Symmetry indicators and anomalous surface states of topological crystalline insulators,” *Phys. Rev. X* **8**, 031070 (2018).

[60] Yadong Jiang, Huan Wang, and Jing Wang, “Monolayer v2mx4: A new family of quantum anomalous hall insulators,” (2023), [arXiv:2303.14685 \[cond-mat.mes-hall\]](https://arxiv.org/abs/2303.14685).

[61] Rui Yu, Xiao Liang Qi, Andrei Bernevig, Zhong Fang, and Xi Dai, “Equivalent expression of \mathcal{Z}_2 topological invariant for band insulators using the non-Abelian Berry connection,” *Phys. Rev. B* **84**, 075119 (2011).

[62] A. A. Burkov and Leon Balents, “Weyl semimetal in a topological insulator multilayer,” *Phys. Rev. Lett.* **107**, 127205 (2011).

[63] Jing Wang, Biao Lian, and Shou-Cheng Zhang, “Dynamical axion field in a magnetic topological insulator superlattice,” *Phys. Rev. B* **93**, 045115 (2016).

[64] Yi Xue Chong, Xiaolong Liu, Rahul Sharma, Andrey Kostin, Genda Gu, K. Fujita, J. C. Séamus Davis, and Peter O. Sprau, “Severe dirac mass gap suppression in sb_2te_3 -based quantum anomalous hall materials,” *Nano Lett.* **20**, 8001–8007 (2020).

[65] Ella O. Lachman, Masataka Mogi, Jayanta Sarkar, Aviram Uri, Kousik Bagani, Yonathan Anahory, Yuri Myasoedov, Martin E. Huber, Atsushi Tsukazaki, Masashi Kawasaki, Yoshinori Tokura, and Eli Zeldov, “Observation of superparamagnetism in coexistence with quantum anomalous hall $c = \pm 1$ and $c = 0$ chern states,” *npj Quantum Materials* **2**, 70 (2017).

[66] M. Garnica, M. M. Otrokov, P. Casado Aguilar, I. I. Klimovskikh, D. Estyunin, Z. S. Aliev, I. R. Amiraslanov, N. A. Abdullayev, V. N. Zverev, M. B. Babanly, N. T. Mamedov, A. M. Shikin, A. Arnau, A. L. Vázquez de Parga, E. V. Chulkov, and R. Miranda, “Native point defects and their implications for the dirac point gap at $\text{mnbi}_2\text{te}_4(0001)$,” *npj Quantum Mater.* **7**, 7 (2022).

[67] Hengxin Tan and Binghai Yan, “Distinct magnetic gaps between antiferromagnetic and ferromagnetic orders driven by surface defects in the topological magnet mnbi_2te_4 ,” *Phys. Rev. Lett.* **130**, 126702 (2023).